Magnetodielectric coupling by exchange striction in Y2Cu2O5

Adem, U.; Nenert, G.; Arramel, [No Value]; Mufti, N.; Blake, Graeme; Palstra, Thomas

Published in:
European Physical Journal B

DOI:
10.1140/epjb/e2009-00209-1

Publication date:
2009

Eur. Phys. J. B **71**, 393–399 (2009)
DOI: 10.1140/epjb/e2009-00209-1

THE EUROPEAN PHYSICAL JOURNAL B

Regular Article

Magnetodielectric coupling by exchange striction in $Y_2Cu_2O_5$

U. Adem[1], G. Nénert[1,2,3], Arramel[1], N. Mufti[1], G.R. Blake[1], and T.T.M. Palstra[1,a]

[1] Zernike Institute for Advanced Materials, University of Groningen, 9747 AG Groningen, The Netherlands
[2] CEA-Grenoble INAC/SPSMS/MDN, 17 rue des martyrs 38054 Grenoble Cedex 9, France
[3] Institut Laue-Langevin, BP 156, 6, rue Jules Horowitz, 38042, Grenoble Cedex 9, France

Received 27 February 2009
Published online 19 June 2009 –

Abstract. We have studied the magnetodielectric response of $Y_2Cu_2O_5$, the so-called blue phase in the Y_2O_3-CuO-BaO phase diagram. Based on symmetry principles, we predict and demonstrate magnetodielectric coupling on a single crystal sample. We report an anomaly in the dielectric constant at the ordering temperature of the Cu spins. We probe the magnetic field-induced phase transitions between four different magnetic phases using magneto-capacitance measurements, demonstrating relatively strong magnetodielectric coupling. We observe an increase in dielectric constant in the spin-flip phase where there exists spontaneous magnetization. We construct a detailed magnetic phase diagram. The magnetodielectric coupling is analyzed in terms of striction induced by symmetric superexchange and optical phonon frequency shifts.

PACS. 77.22.-d Dielectric properties of solids and liquids – 75.80.+q Magnetomechanical and magnetoelectric effects, magnetostriction – 77.80.-e Ferroelectricity and antiferroelectricity – 75.30.Kz Magnetic phase boundaries

1 Introduction

There is at the moment enormous interest in multiferroic and magnetoelectric materials [1]. Ferroelectricity and magnetism seldom coexist, due to the fact that many ferroelectrics need atoms with an empty d-shell for off-centering to occur, whereas magnetism requires partially filled d-shells [2]. Nevertheless, mechanisms for obtaining ferroelectricity that do not involve off-center displacements of transition metal cations have been discovered. Examples are geometric ferroelectrics such as $BaMF_4$ (M = Ni, Co) [3,4] and hexagonal $RMnO_3$ [5], electronic ferroelectricity [6], and magnetically induced ferroelectricity [7,8]. The last discovery has become the focus of research on multiferroics e.g. [9–11], since large coupling is observed between electric and magnetic ordering. Despite the increase in the variety of mechanisms and materials in the study of multiferroic materials, more systems must be studied to understand the microscopic mechanisms involved in magnetoelectric coupling.

Magnetic insulators with a polar space group have the potential to be multiferroic. Not all polar materials are ferroelectric, because this requires that the polarization must be switchable. Therefore, a simple approach for obtaining new multiferroics involves selecting polar magnetic insulators and checking for the presence of ferroelectricity. This approach, however, is rather too exploratory, since there are many pyroelectric materials that are not ferroelectric like $GaFeO_3$ [12] or $TlSeVO_5$ [13]. One can add another condition to focus this exploratory approach: one should look for a polar magnetic insulator that allows the linear magnetoelectric effect by symmetry. This might contribute to larger magnetoelectric coupling compared to that in an ordinary polar magnet since direct coupling between the electrical polarization and magnetization is allowed. The symmetry of the material in the magnetically ordered state determines whether the linear magnetoelectric effect is allowed [14].

Dielectric anomalies are often observed at the magnetic ordering temperature in multiferroic and magnetoelectric materials (irrespective of the type of magnetic ordering). This is the case, for example, in $BaMnF_4$, $YMnO_3$, $BiMnO_3$ and Cr_2O_3, where it is recognized as evidence for magneto(di)electric coupling [3,15–17]. In addition to the terms *linear magnetoelectrics* and *multiferroics*, a third term has recently been introduced to classify certain magnetic materials that possess neither spontaneous polarization nor satisfy the symmetry constraints for the linear magnetoelectric effect, but still show some kind of coupling between the dielectric properties and magnetization. It was first suggested by Lawes et al., who refer to the book by Landau and Lifshitz [18], that

[a] e-mail: t.t.m.palstra@rug.nl

the term *magnetoelectric* should be reserved for special symmetries where a free energy invariant proportional to PM is allowed. They introduced "for more general couplings" the term *magnetodielectric* [19]. We will accordingly use the term *magnetodielectric coupling* instead of *magnetoelectric coupling* for systems that do not allow the linear magnetoelectric effect by symmetry.

Here, we present evidence for magneto(di)electric coupling in a polar antiferromagnet $Y_2Cu_2O_5$, which is well known as the so-called blue phase in the Y_2O_3-CuO-BaO phase diagram [20]. There were three main reasons to choose this compound: (1) the combination of a polar space group and magnetic Cu^{2+} ions make it a potential multiferroic; (2) we have carried out symmetry analysis and concluded that magnetic symmetry allows the linear magnetoelectric effect; (3) it has been established from measurements on many multiferroic and magnetodielectric materials that magnetocapacitance measurements are sometimes able to probe the presence and nature of the magnetic phase transitions even better than magnetization measurements [21–23]. Taking into account that $Y_2Cu_2O_5$ shows two metamagnetic transitions (see below), it is interesting to study these transitions by measuring the dielectric constant, given the high possibility of the magnetodielectric nature of the system.

Recently, linear magnetoelectric coupling was calculated theoretically based on the principle of symmetric exchange striction. In an applied magnetic/electric field, the metal-oxygen bond lengths will change in order to maximize the superexchange interaction [24,25]. Conversely, upon magnetic ordering, the same principle causes changes in the bond lengths/angles in order to maximize the superexchange. For antiferromagnetic superexchange interactions the metal/ligand will displace towards the 180° metal-oxygen-metal bond angle; for ferromagnetic interactions the bond angle will be modified towards 90°.

$R_2Cu_2O_5$ compounds crystallize in the polar orthorhombic space group $Pna2_1$ when R (R being the rare-earth) has an ionic radius smaller than Gd, as well as for Y, Sc and In. The crystal structure, together with a more detailed view of one Cu chain, is depicted in Figure 1. There are two different sites for both Cu and R ions in the unit cell, with very similar coordination. Cu ions have a distorted square planar coordination; there are four O ions within a distance of 1.9 Å, and a fifth at a distance of 2.7 Å. The Cu1 and Cu2 ions are coupled to form dimers, which form Cu_2O_5 zigzag chains along the a axis. The Cu ions in adjacent chains are also connected along the b axis to form ab pseudoplanes. These pseudoplanes are separated by the rare-earth ions, which have a distorted octahedral coordination and are connected in three dimensions [26].

Magnetic ordering in $R_2Cu_2O_5$ systems is complicated, with several exchange interaction paths being present. The magnetic ordering has been studied by neutron diffraction by Garcia-Munoz et al. [27]. At 1.5 K, the magnetic structures are commensurate with the propagation vector $\mathbf{k} = [0, 0, 0]$ for Y, Er and Tm, $\mathbf{k} = [0, 1/2, 0]$ for Ho and $\mathbf{k} = [0, 1/2, 1/2]$ for Yb. The Cu^{2+} moments

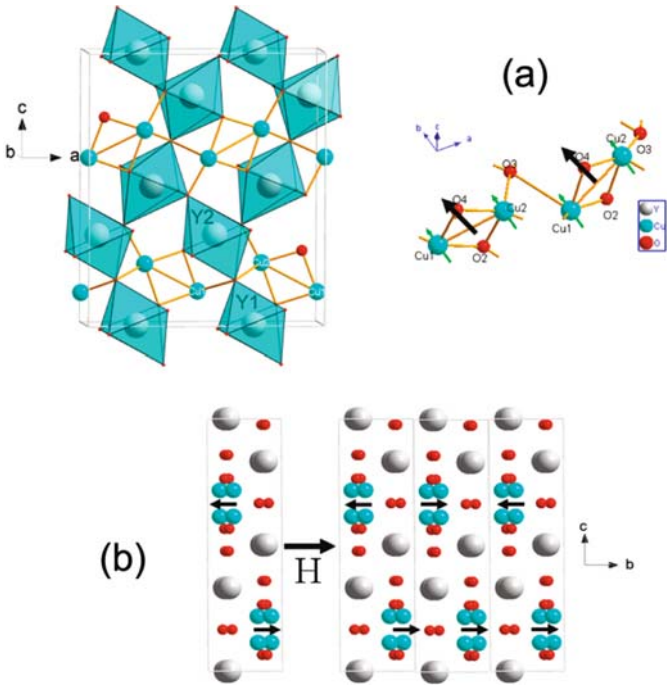

Fig. 1. (Color online) (a) Crystal structure of $Y_2Cu_2O_5$ (left) with a close-up of the copper-oxygen chain along a (right). The black lines denote the S=1 Cu dimer spins oriented along the b axis, (b) Magnetic structure of $Y_2Cu_2O_5$ before and after the spin flip transition modified from [27,28].

are aligned ferromagnetically along the [010] direction in the ab pseudoplanes formed by the Cu chains, and adjacent pseudoplanes are antiferromagnetically (AF) coupled along the c axis. Metamagnetic transitions have been observed in $R_2Cu_2O_5$, first reported by Cheong et al. [20] for a single crystal of $Y_2Cu_2O_5$. In $Y_2Cu_2O_5$ these transitions occur when the magnetic field is applied parallel to the easy-axis, b. At 4.2 K, the first field-induced transition occurs at a critical field of $H_{C1} = 2.8$ T. A second step is observed at $H_{C2} = 4.7$ T, and the magnetization reaches saturation at 7.3 T [28]. A phase diagram has been constructed from anomalies in the magnetization measurements [20]. In this study, we use magnetocapacitance measurements to show that magnetodielectric coupling occurs in $Y_2Cu_2O_5$ single crystals, which we then exploit to perform a detailed study of the field-induced magnetic transitions.

2 Experimental methods

A single crystal of $Y_2Cu_2O_5$ was synthesized using the travelling solvent floating zone technique (TSFZ), following the method of Nishimura et al. [29]. The ratio of Y_2O_3:CuO in our solution rod was 4.6:95.4 [29]. Crystal growth took place only at a slow growth rate of 0.1 mm/h. An atmosphere of 60% Ar : 40% O_2 was used. The growth process lasted for a total of 3 weeks. The upper and lower shafts were both rotated at 20 rpm. The single crystal obtained was 15 mm long and 6 mm in diameter.

A Bruker D8 X-ray diffractometer operating in Bragg-Brentano geometry was used for the powder diffraction of the crushed single crystals. The Single crystal X-ray diffraction (SXD) experiments were performed using a Bruker AXS APEX single crystal diffractometer operating with monochromatized Mo-Kα radiation equipped with a CCD camera. The magnetization M(T,H) of the samples was measured using a SQUID magnetometer (MPMS7 Quantum Design) in applied fields of up to 7 T. The capacitance of the samples was measured using a commercial system (PPMS Quantum Design) with a home-made insert and an Andeen-Hagerling 2500A capacitance bridge operating at a fixed measurement frequency of 1 kHz; the frequency could be varied using an Agilent 4284A LCR meter. A maximum magnetic field of 9 T was applied. Electrical contacts were made using Ag epoxy. The typical thickness of the crystals was 1 mm, with a surface area of 2 by 3 mm. We checked for the presence of a linear magnetoelectric effect by performing pyroelectricity measurements under applied magnetic fields. P-E loops were measured using a Radiant Precision Workstation ferroelectric tester.

3 Results and discussion

3.1 Diffraction

The crystallinity and lattice parameters of our $Y_2Cu_2O_5$ single crystal were checked using powder X-ray diffraction on a crushed single crystal. The lattice parameters, a = 10.8117(23) Å, b = 3.4993(7) Å, and c = 12.4756(26) Å, are slightly different to those in previous reports [26]. Powder diffraction on a crushed piece of the single crystal showed that the sample contained a very small amount of CuO impurity possibly due to contamination from the solution rod. Nevertheless, a good fit was obtained between the observed and calculated diffraction patterns. However, the corresponding fit using single crystal diffraction data was rather poor and the refined atomic parameters had large standard deviations. This was largely attributable to the broadness of the reflections, suggesting that the crystallinity was not perfect.

3.2 Magnetic properties

We first present the results of our magnetization measurements. In Figure 2 magnetic susceptibility measurements along the three different crystallographic axes are presented. A sharp maximum at 12 K is observed, marking a 3D AF ordering as reported previously [20,30,31]. Curie-Weiss fits to the linear regime of the inverse susceptibility measured along the c axis (see the inset of Fig. 2) yield a positive Weiss temperature of 43.5 K, indicating the presence of ferromagnetic exchange interactions [30]. The effective magnetic moment was calculated as 2.75 μ_B per formula unit in agreement with the value reported by Troc et al. [32]. The magnetic anisotropy is small, but the

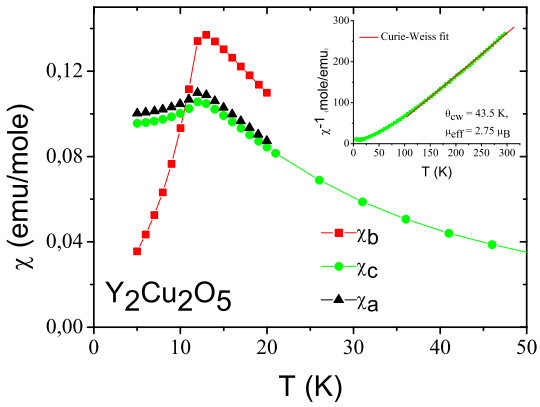

Fig. 2. (Color online) Magnetic susceptibility as a function of temperature, measured for a magnetic field of 0.5 T applied along the three crystal axes. The inset shows the inverse susceptibility measured along the c-axis.

susceptibility along b is larger than that for the other directions, thus b is the easy axis. In Figure 3a, the magnetic susceptibility along the easy axis is plotted for different applied fields. AF ordering is suppressed by a magnetic field, as reported previously [20].

The magnetic field dependence of the magnetization along the three crystallographic axes is also plotted in Figure 3c. Two field-induced transitions are observed, marked by steps in the magnetization, only when the magnetic field is applied parallel to the easy axis, b. Figure 3b also shows how these magnetic transitions evolve with temperature; both transitions become broader on heating, while the critical field for the second transition, H_{c2}, decreases significantly. The critical fields for the two transitions and the maxima in the magnetic susceptibility measurements were previously used by Cheong et al. to construct a magnetic phase diagram [20]. The magnetic phase diagram obtained using our data was very similar, marking the presence of three magnetic phases (Fig. 3d).

The field-induced phase transitions have previously been investigated by neutron diffraction and symmetry analysis [28,33]. The magnetic unit cell in the ground state consists of ferromagnetic Cu pseudolayers stacked in AF fashion along the c axis; the magnetic moments in the layers point along [010]. The first step in the magnetization, interpreted as a spin-flip (metamagnetic transition), coincides with a tripling of the magnetic unit cell along the b axis, which is due to the flip of some of the antiferromagnetically coupled spin dimers along c with the magnetic field (see Fig. 1b) [27,28]. The magnitude of the increase in magnetization corresponds to 1/3 of the saturation magnetization [27]. The second field-induced transition has been interpreted as a spin-flop; the spins rotate such that they all become perpendicular to the field. Upon further increase in magnetic field the spins become aligned in the direction of the field and the magnetic moment is saturated [35]. Figure 1b summarizes the different magnetic structures (adapted from Refs. [27,28]).

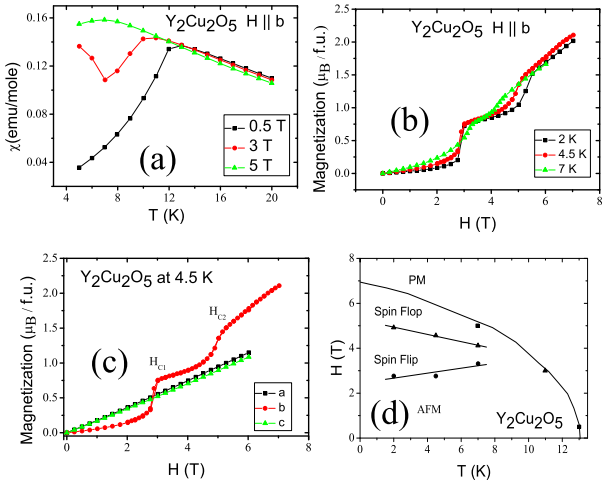

Fig. 3. (Color online) (a) Magnetic susceptibility along the easy axis b for different applied fields. (b) Magnetic field dependence of b-axis magnetization at different temperatures. (c) Magnetic field dependence of magnetization along the three crystallographic axes at 4.5 K. (d) Magnetic phase diagram obtained from magnetization measurements. Thin lines are guides to the eye.

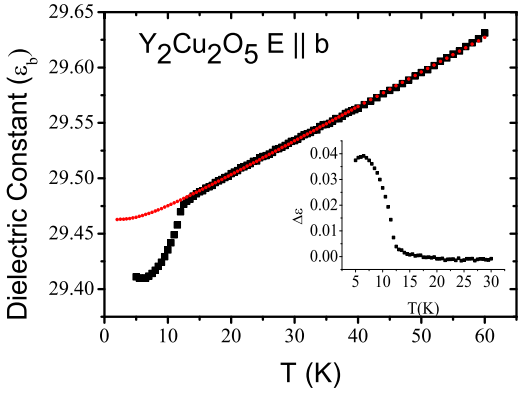

Fig. 4. (Color online) Temperature dependence of the dielectric constant of $Y_2Cu_2O_5$. The red line is a fit to the expression in reference [34]. The inset shows $\Delta\varepsilon$, the change in ϵ_b upon magnetic ordering, which is proportional to the square of the AF order parameter, L^2 (see main text for details).

3.3 Dielectric properties

Within the polar $R_2Cu_2O_5$ family (R = Tb-Lu, Sc, Y and In), the dielectric constant has been reported only for $Er_2Cu_2O_5$, which has a high-frequency (ϵ_∞) value of 9 for polycrystalline samples at RT [36]. We have measured for the first time the dielectric constant of $Y_2Cu_2O_5$ single crystal at low temperatures. All the measurements were performed on crystals oriented along the easy b axis.

The temperature dependence of the dielectric constant of $Y_2Cu_2O_5$ along the b axis is shown in Figure 4. The value of the dielectric constant is approximately 30 at low temperatures; this may differ from the value previously reported for polycrystalline $Er_2Cu_2O_5$ due to the anisotropy of our $Y_2Cu_2O_5$ single crystal. We note that the dielectric constant does not strongly depend on the measurement frequency in the low temperature range where our interest lies. The dielectric loss (tanδ) in this range was smaller than 0.001.

We observe an anomaly in the dielectric constant of $Y_2Cu_2O_5$ at 13.2 K, where AF ordering emerges. Two physical mechanisms might be responsible for this anomaly: magnetostriction and direct polar optical phonon-magnon (magnetoelectric) coupling [37]. Magnetostriction causes the lattice to contract along the direction of the exchange interaction, giving rise to an increase in the phonon energies of modes corresponding to the displacements, and the dielectric constant will decrease according to the LST (Lyddane-Sachs-Teller) equation [37]. In the second mechanism direct magnon-phonon coupling can increase the energy of the lowest frequency transverse optical phonon, decreasing the dielectric constant. Such shifts of the phonon frequencies upon magnetic ordering have been reported for hexagonal $HoMnO_3$ [38] and $GdFe_3(BO_3)_4$ [39]. The temperature dependence of the dielectric constant involves the excitation of low-lying optical phonons. We have fitted the dielectric constant vs. temperature curve to an equation similar to Barrett's equation $\epsilon_b(T) = \epsilon_b(0) + C_0/[\exp(\hbar\omega_0/k_bT) - 1]$ following reference [34]. In this equation, C_0 is a coupling constant and ω_0 is the mean frequency of the final states in the lowest lying optical phonon branch. We obtained values of 0.05 for C_0 and 16 ± 2 cm^{-1} for ω_0. No Raman or infrared studies have been carried out on single crystals of $Y_2Cu_2O_5$, and thus we are unable to say whether the phonon mode obtained from our dielectric constant fits corresponds to any particular Raman or infrared-active phonon in the sample. From studies on polycrystalline samples, the frequency of the lowest lying infrared active phonon is 74 cm^{-1} [40].

The magnetic contribution to the dielectric constant can be modeled using Ginzburg-Landau theory. The free energy contains magnetic and electric terms and also terms that couple the polarization P and the (sublattice) magnetization (L) M. The dielectric constant is obtained by differentiating the equilibrium polarization with respect to the electric field. The lowest-order symmetry-allowed coupling terms are P^2L^2 or P^2M^2 because they leave the free energy invariant with respect to the symmetry operations of the magnetic space group. If both L and M are finite, terms including PLM can also be symmetry allowed for linear magnetoelectric materials [41]. For the multiferroic $YMnO_3$ and $BaMnF_4$ the suppression of the dielectric constant below T_N is thus associated with the emergence of the sublattice magnetization L and is proportional to L^2 [15,42,43]. We show $\Delta\epsilon_b$ as an inset in Figure 5, which behaves like a magnetic order parameter, L^2.

It is revealing to look at both the magnetic field dependence of the capacitance at different temperatures and the temperature dependence of the dielectric constant under different magnetic fields. For convenience, we abbreviate the former as $\epsilon_T(H)$ and the latter as $\epsilon_H(T)$. These measurements differ because $\epsilon_H(T)$ reflects both the temperature dependence and magnetic field dependence of the

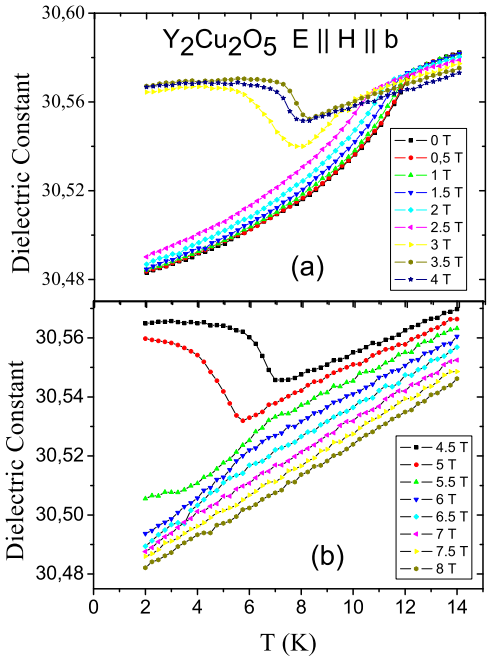

Fig. 5. (Color online) Temperature dependence of the dielectric constant of $Y_2Cu_2O_5$ (a) between 0–4 T (b) between 4.5–8 T.

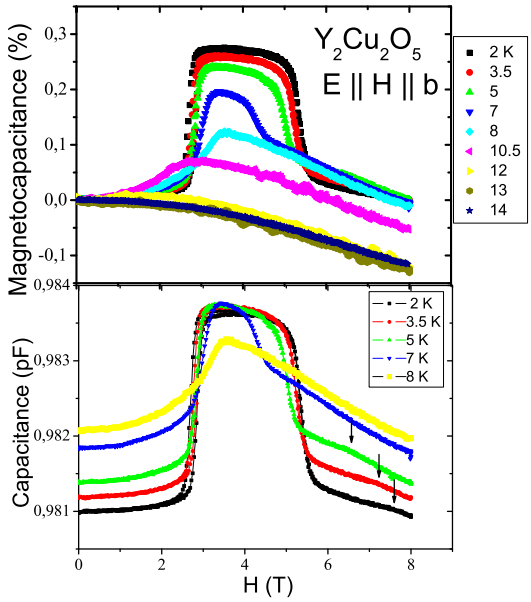

Fig. 6. (Color online) (a) Magnetocapacitance of $Y_2Cu_2O_5$. (b) Unnormalized capacitance vs. magnetic field; arrows indicate the phase transitions from the spin-flop phase into the paramagnetic phase, for $E \parallel b$ and $H \parallel b$.

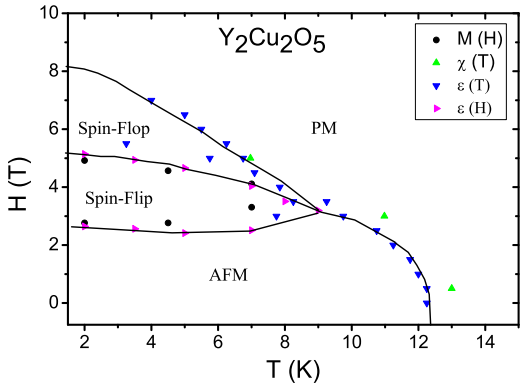

Fig. 7. (Color online) Magnetic phase diagram of $Y_2Cu_2O_5$ obtained using data points from different measurements. The lines are guides to the eye.

lattice polarizability. In contrast, $\epsilon_T(H)$ probes the change in the polarizability with magnetic field only.

In Figure 5a, $\epsilon_H(T)$ is plotted for various magnetic fields of up to 4 T. We observe that magnetic field shifts the dielectric anomaly at T_N to lower temperatures, consistent with the behavior of an antiferromagnet. For $H \geq 3$ T, the dielectric constant first decreases at T_N before a second anomaly corresponding to an increase in the dielectric constant occurs at lower temperatures. This increase in dielectric constant coincides with the field-induced magnetic transition. In Figure 5b, data for fields up to 8 T are shown. We observe that above 5 T, the second anomaly in the dielectric constant vanishes, whereas the first anomaly corresponding to T_N is visible up to 7 T.

Magnetocapacitance measurements (Fig. 6a) at different temperatures better illustrate the relation between the field-induced magnetic transitions and the dielectric constant. At low fields (in the AF phase) and in the paramagnetic phase (not shown in detail), the dielectric constant varies quadratically with magnetic field, which can be explained by a P^2H^2 term in the Landau free energy expression, a term that is allowed independent of the symmetry. The magnetocapacitance in this region is positive below T_N and negative at and above it. When the transition to the spin-flip phase occurs at 3 T, the dielectric constant increases abruptly. Close to 5 T the dielectric constant suddenly decreases as the transition from the spin-flip phase to the spin-flop phase takes place. Above 6 T, the dielectric constant decreases with field in approximately linear fashion. From the unnormalized capacitance versus field curves of Figure 6b, it is possible to observe a change in slope between 6 T and 8 T depending on the temperature, which corresponds to a further transition from the spin-flop phase to the paramagnetic phase. For example, the 5 K data clearly show the presence of four phases along a single curve.

By using the anomalies in the $\epsilon_H(T)$ and $\epsilon_T(H)$ measurements, we have constructed a magnetic phase diagram (Fig. 7) that is in agreement with the phase diagram obtained from the magnetization measurements (Fig. 3d). Moreover, the $\epsilon_H(T)$ and $\epsilon_T(H)$ measurements reveal the phase boundaries in more detail than is possible with magnetization measurements alone.

3.4 Linear magnetoelectric effect and possible ferroelectricity

Analyzing the unit cell and using the existing information on the magnetic structure, one can see that the space

group $Pna2_1$ has magnetic point group $m'm'2$, by applying Bertaut's method [44]. For this magnetic point group, the linear magnetoelectric effect is allowed. According to reference [14] the corresponding magnetoelectricity tensor is

$$\begin{pmatrix} \alpha_{11} & 0 & 0 \\ 0 & \alpha_{22} & 0 \\ 0 & 0 & \alpha_{33} \end{pmatrix}.$$

Therefore, we expect to observe the linear magnetoelectric effect, such that an electrical polarization, P, can be induced under applied magnetic field: $P_i = \frac{\partial \Phi}{\partial E_i} = \alpha_{ij} H_j$. The magnetoelectricity tensor includes the α_{ij} for different directions. In the case of point group $m'm'2$, only the diagonal elements are non-zero. We have measured the magnetoelectric effect along the b axis. We were unable to observe any induced polarization along the b axis, which may be due to insufficient electrical poling or low magnetoelectric coupling, resulting in small induced currents. This (small induced currents-lack of demonstration of the linear magnetoelectric effect) is the case for $GaFeO_3$ [45].

$Y_2Cu_2O_5$ has a polar structure with space group $Pna2_1$, in which the polar axis is c. Therefore, spontaneous electrical polarization can be expected only along this direction. Due to the shape and quality of our crystal, we were unable to measure the polarization along the polar c axis for $Y_2Cu_2O_5$. Therefore, we measured (P-E) hysteresis loops of polycrystalline samples of isostructural $Er_2Cu_2O_5$ and $Yb_2Cu_2O_5$ pellets at room temperature and at lower temperatures. We observed a slight opening of the loop at room temperature for $Er_2Cu_2O_5$, which was due to the lossy character of the sample. At lower temperatures a linear P-E behavior was observed for both the Er and Yb compounds. Therefore, we conclude that $R_2Cu_2O_5$ do not exhibit ferroelectric displacements but pyroelectricity.

3.5 Discussion

With the magnetic phase diagram at hand, it is revealing to look once again at the magnetocapacitance data. One striking point worth emphasizing is the nature of the dielectric anomalies in the different magnetic phases. In the AF phase, a decrease in the dielectric constant at T_N occurs. At 3 T, when the sample is cooled down from 14 K, a decrease in $\varepsilon(T)$ occurs as the AF phase is entered, followed by an increase in $\varepsilon(T)$ at approximately 8 K where the transition to the spin-flip phase occurs. At higher fields, such as 5 T, the sample first enters the spin-flop phase when cooling from 14 K, but no clear anomaly can be seen. When the temperature is further decreased, a transition to the spin-flip phase occurs, which is coincident with an increase in $\varepsilon(T)$. When the sample is cooled from 14 K in a field of 6 T, the spin-flop phase is entered directly and ε decreases. Summarizing these observations, transitions to the ground AF state and the spin-flop state involve a decrease in $\varepsilon(T)$. In the spin-flip phase, there is net magnetization and the dielectric constant increases when the transition to this phase occurs. This increase in $\varepsilon(T)$ is consistent with the field-dependence of the dielectric constant. The dielectric constant is significantly larger in the spin-flip phase than in the other magnetic phases.

It is very unusual to observe an increase in $\varepsilon(T)$ with decreasing temperature. To the best of our knowledge, theoretically there is no prediction for the sign of the dielectric anomalies due to magnetic ordering [34]. One of the rare examples for which such a feature occurs is hexagonal $HoMnO_3$, where the increase in $\varepsilon(T)$ is very sharp, associated with a magnetic phase transition [46]. Magnetocapacitance measurements on this compound also showed an abrupt increase in the dielectric constant when the phase transition was induced. The symmetry of the high-dielectric constant phase in $HoMnO_3$ and the spin-flip phase in $Y_2Cu_2O_5$ have one property in common: the $P6_3$ space group in $HoMnO_3$ allows spin canting and therefore a ferromagnetic component is present [46], just like the spin-flip phase in $Y_2Cu_2O_5$. One could use our results to propose that whenever there is net magnetization, the dielectric constant will increase below the magnetic ordering temperature. However, this proposition would be incorrect; for example, the dielectric anomaly in ferromagnetic $BiMnO_3$ is negative [16].

We attempt to understand the changes in the dielectric constant in terms of displacements associated with superexchange interactions in the different magnetic phases. In the exchange striction model, the metal-oxygen-metal bond angles tend towards 180° with AF exchange, whereas they tend towards 90° for FM exchange. In the spin-flip phase one spin in every second layer reverses, yielding some AFM interactions along the b axis (see Fig. 1b). This spin-flip also changes some of the AF interactions to FM along the c axis. The coupling along the a-axis remains FM [28]. The change of some of the interactions into AF along b axis will according to the exchange striction model result in an increase of the bond angle to accommodate the AF interaction. This expansion of the b-axis will through volume conservation result in a compression of the other two axes. The expansion via the exchange striction model softens the optical phonons along the b axis via the Lyddane-Sachs-Teller (LST) relation. And this will result in an increase of $\varepsilon_b(H)$. We expect that upon the spin-flop transition at 5.5 T the spins revert to FM coupling along the b-axis, as in the magnetic ground state. This corresponds to the decrease in $\varepsilon_b(H)$. In this interpretation, no sharp anomaly is expected at the saturation transition as the spin directions do not change radically, and only the magnetic susceptibility is affected. We note that the interpretation of the neutron diffraction data is not conclusive about the structures of the magnetic phases [28].

4 Conclusion

In conclusion, we have measured the (magneto) capacitance of $Y_2Cu_2O_5$ single crystals and observed different types of anomalies in different magnetic phases. Significant magnetodielectric coupling is demonstrated by anomalies in both the field and temperature dependence

of the dielectric constant, which has allowed us to construct a magnetic phase diagram with higher resolution than that obtained from magnetization measurements. An abrupt increase in the dielectric constant occurs when a large enough magnetic field is applied to cross the phase line into the spin-flip phase. The dielectric constant then suddenly decreases when the field is increased further and the spin-flop phase is entered. We attempt to qualitatively understand these changes by considering that the magnetic superexchange interaction changes sign at both phase transitions, leading to changes in the corresponding Cu-O-Cu bond angles which induces shifts in the optical phonon frequencies. We conclude that optical phonon frequency shifts (via the LST relation) due to striction in the magnetic phases are effective in determining the changes in ε. Further studies about the details of the magnetic structure as well as optical phonon spectroscopy are necessary to substantiate this interpretation.

We thank Jacob Baas for experimental help and Auke Meetsma for SXD. This work is funded by the Stichting FOM (Foundation for Fundamental Research of Matter), and by the Dieptestrategie of NWO (Dutch National Science Organization).

References

1. S.W. Cheong, M. Mostovoy, Nature **6**, 13 (2007)
2. N.A. Hill, J. Phys. Chem. B **104**, 6694 (2000)
3. J.F. Scott, Rep. Prog. Phys. **12**, 1055 (1979)
4. C. Ederer, N.A. Spaldin, Phys. Rev. B **74**, 024102 (2006)
5. B.B. Van Aken, T.T.M. Palstra, A. Filippetti, N.A. Spaldin, Nature Materials **3**, 164 (2004)
6. N. Ikeda et al., Nature **436**, 1136 (2005)
7. T. Kimura, T. Goto, H. Shintani, K. Ishizaka, T. Arima, Y. Tokura, Nature (London) **426**, 55 (2003)
8. M. Mostovoy, Phys. Rev. Lett. **96**, 067601 (2006)
9. T. Kimura, Y. Sekio, H. Nakamura, T. Siegrist, A.P. Ramirez, Nat. Mater. **7**, 291 (2008)
10. T. Kimura, J.C. Lashley, A.P. Ramirez, Phys. Rev. B. **73**, R220401, (2006)
11. Y. Yamasaki, S. Miyasaka, Y. Kaneko, J.-P. He, T. Arima, Y. Tokura, Phys. Rev. Lett. **96**, 207204 (2006)
12. N. Kida, Y. Kaneko, J.P. He, M. Matsubara, H. Sato, T. Arima, H. Akoh, Y. Tokura, Phys. Rev. Lett. **96**, 167202 (2006)
13. T. Sivakumar, H.C. Chang, J. Baek, P.S. Halasyamani, Chem. Mater. **19**, 4710 (2007)
14. *International Tables for Crystallography, Physical Properties of Crystals*, edited by A. Authier (Kluwer Academic Publishers, 2003), Vol. D
15. A.A. Nugroho, N. Bellido, U. Adem, G. Nénert, C. Simon, M.O. Tija, M. Mostovoy, T.T.M. Palstra, Phys. Rev. B **75**, 174435 (2007)
16. T. Kimura, S. Kawamoto, I. Yamada, M. Azuma, M. Takano, Y. Tokura, Phys. Rev. B **67**, 180401 (2003)
17. H.B. Lal, R. Srivastava, K.G. Srivastava, Phys. Rev. **154**, 505 (1967)
18. L.D. Landau, E.M. Lifshitz, L.P. Pitaevskii, Electrodynamics of Continuous Media (Pergamon, New York, 1984)
19. G. Lawes, A.P. Ramirez, C.M. Varma, M.A. Subramanian, Phys. Rev. Lett. **91**, 257208 (2003)
20. S.W. Cheong, J.D. Thompson, Z. Fisk, K.A. Kubat-Martin, E. Garcia, Phys. Rev. B **38**, 7013 (1988)
21. U. Adem, M. Mostovoy, N. Bellido, A.A. Nugroho, C. Simon, T.T.M. Palstra, e-print `arXiv:0811.4547`
22. T. Katsufuji, H. Takagi, Phys. Rev. B **64**, 054415 (2001)
23. N. Bellido, C. Simon, A. Maignan, Phys. Rev. B **77**, 054430 (2008)
24. N.A. Spaldin, M. Fiebig, M. Mostovoy, J. Phys.: Condens. Matter **20**, 434203 (2008)
25. K.T. Delaney, M. Mostovoy, N.A. Spaldin, Phys. Rev. Lett. **102**, 157203 (2009)
26. J.L. Garcia-Munoz, J. Rodriguez-Carvajal, J. Solid State Chem. **115**, 324 (1994)
27. J.L. Garcia-Munoz, J. Rodriguez-Carvajal, X. Obradors, M. Vallet-Regi, J. Gonzales-Calbet, M. Parras, Phys. Rev. B **44**, 4716 (1991)
28. Y. Matsuoka, Y. Nishimura, S. Mitsudo, H. Nojiri et al., J. Magn. Magn. Mater. **177–181**, 729 (1998)
29. Y. Nishimura, Y. Matsuoka, S. Miyashita, H. Komatsu, M. Motokowa, T. Nakada, G. Sazaki, J. Crystal Growth **207**, 206 (1999)
30. R. Troc, J. Klamut, Z. Bukowski, R. Horyn, J. Stepien-Damm, Physica B **154**, 189 (1989)
31. B.L. Ramakrishna, E.W. Ong, Z. Iqbal, Solid State Commun. **68**, 775 (1988)
32. R. Troc, Z. Bukowski, R. Horyn, J. Klamut, Phys. Lett. A **125**, 222 (1987)
33. J.L. Garcia-Munoz, X. Obradors, J. Rodriguez-Carvajal, Phys. Rev. B **51**, 6594 (1995)
34. D.L. Fox, D.R. Tilley, J.F. Scott, H.J. Guggenheim, Phys. Rev. B **21**, 2926 (1980)
35. B. Lebech, Y. Matsuoka, K. Kakurai, M. Motokowa, Progress of the Theoretical Physics Supplement **150**, 222 (2005)
36. G. Knebel, P. Lunkenheimer, A. Loidl, G. Wltschek, H. Fuess, J. Alloys and Compounds **216**, 99 (1994)
37. G.A. Samara, J.F. Scott, Solid State Commun. **21**, 167 (1977)
38. A.P. Litvinchuk, M.N. Iliev, V.N. Popov, M.M. Gospodinov, J. Phys.: Condens. Matter **16**, 809 (2004)
39. D. Fausti, A.A. Nugroho, P.H.M. Van Loosdrecht, S.A. Klimin, M.N. Popova, L.N. Bezmaternykh, Phys. Rev. B **74**, 024403 (2006)
40. Z.V. Popovic, C. Thomsen, M. Cardona, R. Liu, G. Stanisic, W. Konig, Z. Phys. B: Condensed Matter **72**, 13 (1988)
41. P. Toledano, Ferroelectrics **161**, 257 (1994)
42. D.L. Fox, D.R. Tilley, J.F. Scott, H.J. Guggenheim, Phys. Rev. B **21**, 2926 (1980)
43. G. Nénert, U. Adem, E.M. Bauer, C. Bellitto, G. Righini, T.T.M. Palstra, Phys. Rev. B **78**, 054443 (2008)
44. E.F. Bertaut, Acta Crystallographica A **24**, 217 (1968)
45. T. Arima, D. Higashiyama, Y. Kaneko, J.P. He, T. Goto, S. Miyasaka, T. Kimura, K. Oikawa, T. Kamiyama, R. Kumai, Y. Tokura, Phys. Rev. B **70**, 064426 (2004)
46. B. Lorenz, A.P. Litvinchuk, M.M. Gospodinov, C.W. Chu, Phys. Rev. Lett. **92**, 087204 (2004)